5-2021

An Eulerian Perspective on Spring Migration in Mule Deer

Tatum Del Bosco
Utah State University

AN EULERIAN PERSPECTIVE ON SPRING MIGRATION IN MULE DEER

by

Tatum Del Bosco

A thesis submitted in partial fulfillment
of the requirements for the degree

of

MASTER OF SCIENCE

in

Ecology

Approved:

_____	_____
Tal Avgar, Ph.D. Major Professor	Jerod Merkle, Ph.D. Committee Member
_____	_____
Julie Young, Ph.D. Committee Member	D. Richard Cutler, Ph.D. Interim Vice Provost of Graduate Studies

UTAH STATE UNIVERSITY
Logan, Utah

2021

ABSTRACT

An Eulerian Perspective on Spring Migration in Mule Deer

by

Tatum Del Bosco, Master of Science

Utah State University, 2021

Major Professor: Dr. Tal Avgar
Department: Wildland Resources

Many ungulate populations follow seasonal migration patterns, residing in low-elevation regions during winter and travelling to high-elevation locations in the summer. Plant phenology also follows elevation gradients, with vegetation at lower elevations undergoing spring green-up earlier in the season. Previous research has demonstrated that, at the individual level, ungulate migration often coincides with this vegetation green-up, a behavior that is hypothesized to allow animals to increase energy uptake by following peak forage quality across the landscape. However, it is still unknown whether these individual level patterns scale up to the population level, and the relative effects of biomass quantity versus quality are still unclear. I utilized novel methods to obtain finely resolved estimates of mule deer (*Odocoileus hemionus*) densities across space and time using camera traps placed across a wide elevation gradient in central Utah. I then used these estimates to test the hypothesis that population-level migration is driven by spring vegetation green up, measured using remotely-sensed indices of biomass availability. My results indicate that deer spring migration in my study area is driven by both forage quantity and quality, and that the wave of vegetation regrowth advancing from low to

high elevation during the spring is closely tracked by a traveling wave of peak deer densities. My study thus provides not only a novel technique to quantify wildlife density dynamics at high spatiotemporal resolution, but also the first demonstration of population-level green-wave surfing.

(57 pages)

PUBLIC ABSTRACT

An Eulerian Perspective on Spring Migration in Mule Deer

Tatum Del Bosco

Many herbivores travel between low-elevation winter ranges and high-elevation summer sites. These seasonal movements allow them to avoid deep snow cover, ensure access to favorable habitat, and maximize food intake throughout the year. During the spring season, plants at lower elevations green up earlier at lower elevations than at higher elevations. It has been shown that individual animals will track this vegetation growth during their spring migration, which allows them to maximize forage intake coming out of the nutrient scarce winter. This phenomena has previously been studied by monitoring individual movement trajectories, but it is unknown how this pattern scales up to the population level. I used trail cameras placed along migration paths to monitor a population of mule deer (*Odocoileus hemionus*) in Central Utah during the spring 2019 season. We quantified fine-scale changes in plant phenology through space and time using remotely-sensed indices of vegetation growth and availability. In my study system, mule deer density was positive correlated with vegetation green-up, providing the first demonstration of this phenomena at the population level.

ACKNOWLEDGMENTS

I would first like to thank my advisor, Tal Avgar, for choosing me as his first graduate student. With your support and mentoring, I've blossomed from a volunteer cleaning tanks of algae to a young wildlife ecologist.

This research wouldn't have been possible without the help of Steven Handtke, who worked tirelessly with me in the field for over two years. I'd like to acknowledge Brian Smith for all of his help and support in my last semester, and Aidan Beers for picking up the phone whenever I needed it.

In no particular order, I'd also like to thank Randall McBride, Lauren Ricci, Kylie Sinclair, Andrew Sharp, Aimee Van Tatenhove, Kezia Manlove, and Clark Rushing.

Finally, I am forever grateful for my family - Tara Del Bosco, Miles Smith, Max Smith, and Honeybear - for their unwavering support and unconditional love.

Tatum Del Bosco

CONTENTS

Page

LIST OF TABLES

Page

LIST OF FIGURES

Page

INTRODUCTION

Many ungulate populations follow distinct altitudinal migration patterns, moving from low elevation winter ranges to high elevation summer sites. Although seasonal migration movement can be energetically costly, it provides essential services to individuals (Avgar et al. 2014, Robbins and Hanley 2016). At the most basic level, travelling to lower elevation winter ranges allows ungulates to avoid deep snow cover that inhibits movement, limits access to bedding and foraging resources, and conducts body heat away from individuals (Monteith et al. 2011). Travelling to summer grounds is also of high importance to pregnant females – spring migration typically coincides with the onset of fawning season in the third trimester, when maternal energy requirements are at their highest (Long et al. 2009, Pettorelli et al. 2005). More generally, travelling between elevation ranges allows ungulates to ensure availability of nutritional resources throughout the year. In the spring months, populations are coming out of a physiologically stressful season during which they have been subjected to metabolically intense temperatures and scarce nutritional resources, and therefore require immense amounts of forage to replenish their depleted body condition (Albon and Langvatn 1992, Fryxell and Sinclair 1988). In summary, seasonal altitudinal migration patterns are an essential adaptation of ungulate populations that exist in harsh climates and landscapes characterised by predictable spatiotemporal variation in resource availability. By travelling between distinct seasonal ranges, individuals are able to increase fitness, with obvious consequences to population viability (Fryxell and Sinclair 1988). Understanding the drivers and associated costs and benefits of seasonal migration is thus crucial for effective management and conservation of migratory populations.

The forage maturation hypothesis states that peak nutritional quality occurs at an intermediate stage of vegetation growth (Fryxell and Sinclair 1988). Early in the growing season, nutritional gains are limited by biomass availability, but as plants mature they become more woody (hence, less digestible) and develop secondary compounds that can increase costs of digesting plant matter (Fryxell and Sinclair 1988). Therefore, foraging on plants at an intermediate growth stage allows herbivores to maximize nutritional uptake by striking a balance between biomass quantity and nutritional quality. In temperate regions, seasonal changes in plant phenology follow an altitudinal pattern (Hebblewhite et al. 2008). Vegetation at lower elevations emerge and experience peak rates of growth earlier in the season than vegetation at higher elevations due to differences in temperature, snow melt, and precipitation. Previous research has demonstrated that ungulate migration often coincides with this vegetation green-up across elevation gradients (Aikens et al. 2020, Bischof et al. 2012, Hebblewhite et al. 2008, Merkle et al. 2016a).

The 'green-wave surfing' hypothesis (GWSH; an offshoot of the more general forage maturation hypothesis), postulates that large herbivores track resource phenology through space, and has been investigated in several study systems and species, including mule deer (*Odocoileus hemionus*), roe deer (*Capreolus capreolus*), red deer/elk (*Cervus elaphus*), moose (*Alces alces*), bighorn sheep (*Ovis Canadensis*), and bison (*Bison bison*) (Aikens et al. 2017, Bischof et al. 2012, Merkle et al. 2016b, Middleton et al. 2018). These studies tested the GWSH using individual-level trajectories (from GPS transmitters) with metrics of forage biomass availability and growth rate derived from remotely-sensed products. Overall, these studies concluded that animals often follow an

emergent wave of green vegetation across the landscape, maximizing energy uptake and allowing them to replenish depleted reserves from the metabolically taxing winter season (Bischof et al. 2012, Merkle et al. 2016b). In turn, this behavior increases individual body fat levels, a crucial factor in determining reproductive capacity (Couturier et al. 2009, Middleton et al. 2018). However, there has been some variability in the findings of these studies. Herbivores in some systems have been found to 'jump' the green wave, travelling ahead of peak forage growth and quickly advancing to their summer range, and others have been found to track biomass availability rather than maximal rate of growth (Bischof et al. 2012, Merkle et al. 2016b). 'Jumping' the green wave can ensure that animals reach fawning grounds and have access to peak vegetation growth, while tracking biomass provides a greater short-term nutritional benefit. NDVI has been found to have a positive effect on animal condition, evidenced by body-fat studies and fecal nitrogen surveys (Lendrum et al. 2014, Middleton et al. 2018).

Despite extensive research of the GWSH at the individual level, such studies are often limited in sample size (as they rely on capturing and collaring individual animals), and it is yet unknown whether this pattern scales up to the population level. Additionally, taking an individual-level approach can make studies susceptible to errors sourced from spatial variability (Martin et al. 2005). The ramifications are that much uncertainty remains regarding the functional role of spring migration in temperate large herbivores, as well as the potential impacts movement barriers and climatically driven phenological shifts may have on this functionality.

One solution to this problem may come from examining migration from a different perspective. Examinations of animal movement patterns can take different

approaches related to physical theories in observing fluid motion patterns (Phillips et al. 2019, Turchin 2015). The Lagrangian perspective refers to how individual particles flow through space and time. In our context, this is akin to observing a single animal's movement trajectory (i.e., using telemetry/GPS data). By contrast, an Eulerian perspective focuses on the entire flow field at a specific location – it is place-based rather than individual based. Linking these two complementary perspectives is arguably a critical aspect of understanding and predicting animal movement patterns, yet the Eulerian perspective is rarely used by wildlife movement ecologists (Phillips et al. 2019, Turchin 2015). Lack of wildlife research using the Eulerian perspective likely stems from technical challenges in collecting Eulerian data at fine spatiotemporal scales (Phillips et al. 2019, Turchin 2015). By contrast, it is much simpler to take a Lagrangian (individual-level) perspective and closely examine the movements of individual animals. The Lagrangian perspective offers greater resolution and can encompass a greater geographical range (such as the entire annual range of an individual), but may not be representative of population-level redistribution patterns (Phillips et al 2019). My research is aimed at building upon existing Lagrangian understanding of ungulate migration while providing an Eulerian perspective that investigates the flow of animal density through space and time.

Eulerian data could be obtained using wildlife camera traps. In recent years, non-invasive wildlife monitoring devices, including camera traps, have risen in popularity for investigating a variety of ecological processes (Burton et al. 2015). These technologies provide an alternative to individual-level tracking and traditional survey techniques, and also allow for larger samples sizes due to their relatively low cost (Kays et al. 2020,

Rovero et al. 2013). Traditionally, camera trapping research has focused on questions related to species occupancy, or, if animals are individually identifiable, abundance (e.g., mark-resight studies) (Burton et al. 2015, Meek et al. 2014). However, recent research has demonstrated that camera trap data can be used to derive estimates of animal density for unmarked animals (Garland et al. 2020, Nakashima et al. 2018). Using encounter rates (i.e., how often an animal is observed) and residence times (i.e., amount of time animals spend in the camera's field of view), it is possible to produce unbiased estimates of animal density specific to the cameras' location and operating time (Garland et al. 2020, Nakashima et al. 2018, Rowcliffe et al. 2008). Here, I used camera trapping to examine daily population redistribution patterns through space and time. Specifically, I used over a hundred cameras that were spread across a 50,000-hectare study area in central Utah, encompassing summer and winter mule deer ranges, from early spring to mid summer.

Mule deer are an abundant ungulate species native to the intermountain west. In mountainous habitats, like those found in our study system, they often display seasonal migration patterns (Nicholson et al. 1997, Sawyer et al. 2005). The current study provides a novel investigation of mule deer spatial redistribution dynamics as they travel from winter to summer ranges, specifically focusing on how availability of limited foraging resources affects migration at the population-level. I utilized photos collected by motion-triggered cameras to track population redistribution dynamics during the spring migration season by quantifying how local mule deer density changed across space and time. These data were then coupled with spatially and temporally dynamic remote-sensed products

used to quantify vegetation availability and growth, to evaluate how the travelling wave of deer density advanced up an elevation gradient, relative to the green wave of forage.

RESEARCH OBJECTIVES

This research evaluates alternative drivers of deer redistribution patterns during the spring migratory season, and has two main objectives. First, I aim to evaluate whether mule deer spring migration in my study area is driven by plant phenology tracking (green-wave surfing), and, if so, the relative importance of forage biomass availability versus growth. Second, I aim to demonstrate a novel approach to mapping animal distributions at fine spatiotemporal scales using camera traps, an approach that could potentially enable a much-needed Eulerian perspective on a variety of questions in wildlife spatial ecology.

I hypothesize that access to high quality forage is the main driver behind spring migration in my study system, as mule deer come out of the metabolically intensive, nutritionally scarce winter season. Under this hypothesis, I expect mule deer migration to track the progression of herbaceous vegetation green up (i.e., forage quality rather than quantity). It is thus predicted that, at the population level, waves of deer density will generally track peak rates of green-up across space and time. A plausible alternative hypothesis is that deer migration is driven purely by forage biomass availability (i.e., quantity rather than quality), under which I predict that deer density will track the local abundance of green herbaceous vegetation rather than its temporal derivative – the growth rate.

FIELD METHODS

Study Area

I conducted this study in Spanish Fork Canyon in Central Utah, in the Uinta National Forest. The area is home to a large mule deer population, which local wildlife managers estimate to be about 5,000 individuals, as well as several other large herbivore species, including elk and moose populations. Local predator species include cougars *(Puma concolor)*, black bears *(Ursus americanus)*, and coyotes *(Canis latrans)*. The region is home to multiple USDA Forest Service grazing allotments, which are occupied by cattle and sheep herds in summer months. The area is frequented by recreationists, including hunters, hikers, and campers.

The study region is composed of mountainous terrain, with elevation gradients ranging from ~1,000 m at the canyon floor to peaks of over 3,000 m, that provide clear elevational gradients and distinct summer/winter ranges for mule deer (Fig. 1). The climate is semi-arid, experiencing hot summers and significant snowfall at high elevations in the winter months. The 50,000-hectare study region is dominated by sagebrush steppe habitat. Commonly occurring vegetation species includes basin sagebrush (*Artemisia tridentate),* scrub oak (*Quercys gambelii*), juniper (*Juniperus scopulorum*), and aspen (*Populus tremuloides*), while higher elevation sites are often characterized by coniferous species.

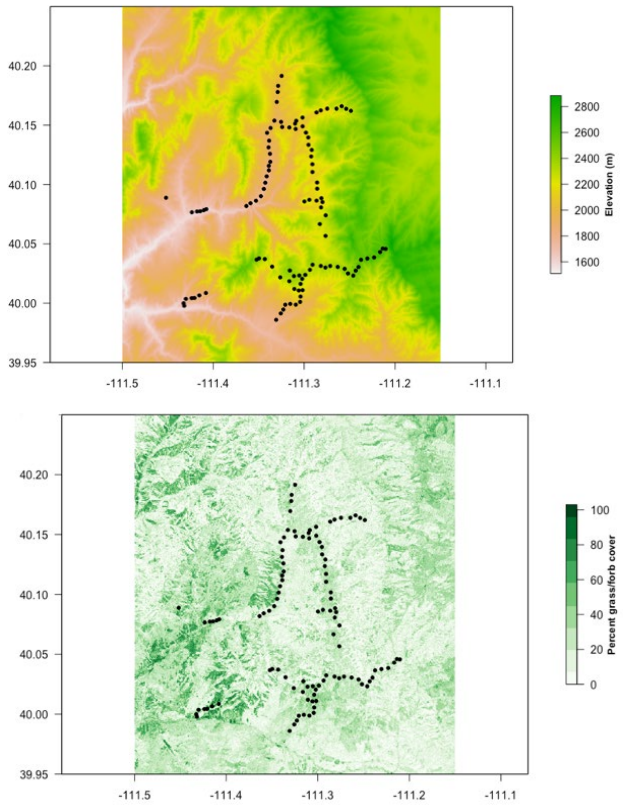

FIG 1. (Left) Elevational map of study area. (Right) Percent grass/forb cover across the study area (based on RAP data; see below for more details). In both maps, site locations are represented by black dots.

General study area selection was informed using mule deer GPS collar data collected by the Utah Division of Wildlife in previous years (https://wildlifemigration.utah.gov/land-animals/tracking/). Within the 50,000 hectare study region however, exact camera locations were randomly placed. In early 2019, I established 106 field sites across an elevation gradient of 1,300 m to 2,600 m in order to encompass both summer and winter mule deer ranges, and to fully sample environmental variability throughout the study area (Fig. 1). I equipped each field site with a trail camera (either Cuddeback H-1453 or Reconyx HP2X) programmed to take photos continuously when motion was detected in its field of view. A uniform 21-m^2 sampling

area was delineated in front of each camera using three metal conduits, placed upright in the ground 9 m from the camera and along a 30-degree arc (Fig. 2).

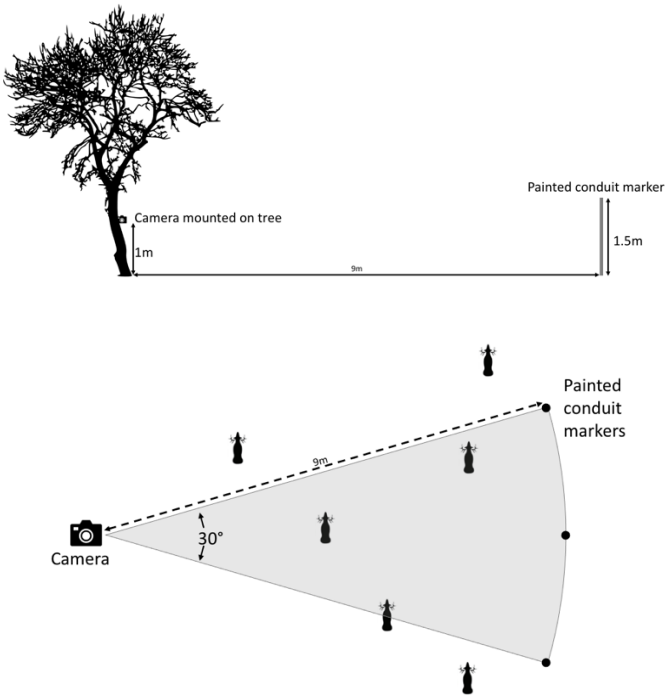

FIG 2. (Left) Illustration of camera setup at a field site and overhead diagram of a field site (right). Note locations of conduit markers and shaded effective sampling area.

Cameras were deployed on a rolling basis throughout the winter and spring months (March – May) in an effort to fully capture spring migration movements, and were spaced a minimum of 1000 m apart to ensure they each occupied unique MODIS NDVI pixels (one of our predictors – see below). For complete deployment protocols, see Appendix B. Sites were revisited in late summer 2019 to collect photos from cameras and to conduct site-level vegetation surveys to assess cover and frequency of forage types. Over 500,000 photos were captured during the 2019 spring migration season, 8% of

which contained images of animal subjects (92% false positives, primarily due to vegetation shifting in the wind).

Extracting data from camera photos

Photos were imported from individual SD cards, and then underwent preliminary processing. They were each assigned a unique file name that included a string specifying the field site they were collected, the SD card they originated from, and when they were collected. Additionally, the photos themselves all contained a band at the bottom of the picture that denoted the site, date, and time they were collected as an additional layer of quality control. All files were backed up to a cloud storage system (Google Drive) as well as a local hard drive.

Once uploaded, photos were sorted and classified by one of four trained technicians. Technicians were initially given a set of 300 training photos to classify, which were then compared to the true classifications identified by the project lead. Before training, technicians had an average misclassification rate of under 10%; classification errors most frequently occurred in close-up photos where the entire animal body was not visible. Technicians repeated the training set until they could correctly identify all photos, and were then allowed to work on the dataset, using the software Wild.ID version 0.9.31 (Nandigam and Fegraus 2018) to view and annotate photos. This interface provided a simple, consistent method for multiple technicians to work with simultaneously, and also automatically extracted metadata from the photo files (date, time, flash, temperature, and site number). I checked datasheets periodically to conduct quality control and investigate outliers. Photos were sorted into broad categories first – ‘blank’ (no animal), ‘misfire’ (a defective/faulty camera), ‘setup’ (photos taken of personnel during camera maintenance),

or ‘animal’. All animals that were captured in photos were counted and identified to the species level, and were classified based on whether they were between or outside of the metal conduits in the photos. For animals that did not clearly appear in in or outside the conduit markers, a 50% rule was used (if more than half of the animal body was inside the markers, it was counted as such). For the analysis described here, data include only photos with mule deer present between the conduit markers and the camera. When describing livestock presence throughout the spring season, we included cattle and sheep presence both inside and outside the markers, as we were interested in the effect of livestock presence and not concerned about calculating density for these species (see below). See Fig. 3, below, for examples of common scenarios encountered in camera trap photos and how they were classified.

FIG 3. Examples of typical scenarios encountered in camera trap photos. Top left shows a deer within conduit markers (sampling area). Top right shows multiple deer outside the markers. Bottom left illustrates cattle inside and outside markers, bottom right is 'blank' and contains no animals (likely triggered by moving vegetation).

Managing such an extensive field study came with a few data management issues. One of the camera models, the Cuddeback H-1453 units, were prone to malfunctioning in two different ways. Firstly, a subset of the Cuddeback cameras were found to be defective in that once activated, they would take continuous photos - regardless of how they were programmed - until either the camera batteries or SD card storage were depleted. Photos collected from these defective cameras overwhelmingly consisted of 'blank' images with no animals. I tagged all of these photos in the method described

above, however, data from these sites was temporally limited, as the cameras typically stopped working within a few hours of deployment.

A second camera data issue was a little more complex. During cold weather events, some of the cameras would turn off, presumably because their batteries froze. When the ambient temperature increased, the cameras would power back on, but would retain the timestamp of when they turned off. I had no way of knowing how long the cameras were powered off for, and consequently, did not know the actual time/date that photos were taken after these freezing periods. I identified these events by manually sifting through all photos taken at sites and checking whether the time stamps seemed appropriate – after a freeze event, the cameras would display a 'night' time (after sunset) on photos that were clearly taken in broad daylight. The date of these malfunctions was noted for afflicted cameras, and all data from photos taken after these dates was discarded.

Quantifying vegetation availability

As my focus here is on the temporally dynamic process of migration, I characterised daily vegetation quantity and quality at each site using remotely sensed NDVI (Normalized Difference Vegetation Index) from MOD09QI surface reflectance data, obtained at an 8-day, 250 m resolution. These data were processed using standard method for quantifying landscape-scale phonological patterns in green wave surfing studies (Merkle et al. 2016b). Briefly, I fit a double logistic curve to the times series of NDVI values for each MODIS pixel in my study area, and used interpolated NDVI from this curve to represent forage quantity in my analysis. I calculated the first derivative of this curve to obtain the instantaneous rate of green-up (IRG), which I used as our measure

of vegetation quality, as was done in several previous studies (Aikens et al. 2020, Bischof et al. 2012, Merkle et al. 2016b). I used the MODIS 'snow flag' to characterize snow presence/absence at each field site. Sites were flagged as 'snow' on any given day if both the current and previous 8-day window were flagged as 'snow' in the MODIS data. If the current 8-day window was not flagged as 'snow', but the previous one was, the first four days were flagged as 'snow' (a linear interpolation).

Site-level vegetation composition was obtained using BLM/NRCS Rangeland Analysis Platform (RAP) data (Boswell et al. 2017). This resource provided percent cover of annual forbs and grasses, perennial forbs and grasses, shrubs, trees, and bare ground at a 30m spatial resolution (Fig. 1). I tested the correlation between my site-level vegetation surveys and these remote-sensed values, and found that the two were positively and linearly correlated (Appendix C). Elevational data for the study area was derived from USGS 'The National Map' resource (USGS 2020).

ANALYTICAL METHODS

The main quantity of interest in this analysis is deer density (deer/area). Individual deer identity was not considered – the same deer may or may not have been observed in multiple photos on the same day. The random encounter and staying time (REST) model, proposed by Nakashima et al. (2018), suggests that animal density can be estimated based on trapping rates and residence times observed from camera trap surveys. When implementing this model, our variable of interest is the amount of time animals spend in the camera's field of view – for example, one animal spending an hour in a sampling area is equivalent to 60 animals spending one minute in the sampling area while for the other 59 minuets the area is unoccupied - both would result in the same estimate of density. In our case, density at each site for a given time period can be calculated as:

$$\rho_{i,t} = N_{i,t} \cdot \frac{\tau_i}{T_{i,t} \cdot A_i}$$

Here, $\rho_{i,t}$ is deer density (in deer/area) in site *i* on day *t*. $N_{i,t}$ is a latent random variable representing the detection-corrected number of deer captured within our sampling area A_i at camera *i* on day *t* (A_i = 21 m^2 for all sites on all days). τ_i is camera recovery time, which is the amount of time from when a photo is taken to when the camera is ready to take another photo if triggered. Through field testing, τ_i was measured to be 2 seconds for both camera models used in this study. Finally, $T_{i,t}$ is the total time (in seconds) that the camera was active and able to take photos if triggered on day *t* (24*60*60 = 86,400 seconds).

I statistically estimated $N_{i,t}$ using a Bayesian hierarchical model. $N_{i,t}$ was modeled as a Poisson random variable with intensity $\lambda_{i,t}$, which was composed of three processes: an occupancy process to model whether a site is used by deer on a given day ($z_{i,t}$), a count process to model the expected number of deer captured in photos given that the site was occupied and assuming perfect detectability ($w_{i,t}$), and a spatiotemporal autocorrelation process $(x_{i,t})$ with reltive importance governed by a linear operator, r ($\in [0, 1]$). Finally, a binomial detection process gave rise to the observed data ($y_{i,t}$), conditioned on $N_{i,t}$. Thus, the model can be written as:

$$N_{i,t} \sim Poisson(\lambda_{i,t}),$$

$$\lambda_{i,t} = [1 - r] \cdot z_{i,t} \cdot w_{i,t} + r \cdot x_{i,t},$$

$$y_{i,t} \sim Binomial(N_{i,t}, p_{i,t}).$$

The occupancy model captures the effect of spatial and temporal predictors on the probability, $\psi_{i,t}$, that a given site is used by deer on a given day. It takes the form of a mixed-effects logit model, with site ID as a random effect on the intercept (hence accommodating site-level variations around the baseline probability of occupancy). The model included, in addition to the intercept, seven predictors (fixed effects; see Table 1). To accommodate the null hypothesis that migration is simply driven by a change in preferred elevation through time, the model included elevation, elevation squared, and their interactions with Julian day. To accommodate the hypotheses that occupancy patterns also change through space and time based on local site attributes, I have also included snow presence/absence (obtained from MODIS snow flags at 8-day resolution) as deer are often thought to prefer snow-free sites, livestock presence/absence (obtained

from camera trap images) as deer are often thought to avoid livestock, and RAP- derived precent tree cover (deer are often thought to avoid densely treed areas). Hence, my occupancy model was designed to capture the effects of all major drivers of deer spatiotemporal distribution, excluding dynamical vegetation patterns. The occupancy process can be written as:

$$z_{i,t} \sim Bernoulli(\psi_{i,t}),$$

$$logit(\psi_{i,t}) = \boldsymbol{X}_{\psi}\boldsymbol{\Gamma} + \eta_i^{\psi},$$

$$\eta_i^{\psi} \sim Normal(0, \sigma_{\psi}),$$

where $\boldsymbol{X}_{\psi}$ is the matrix of predictor variables, $\boldsymbol{\Gamma}$ is the vector of regression coefficients, and η_i^{ψ} is the site-level random effect with standard deviation σ_{ψ}.

The abundance model included covariates that could potentially affect deer density in a given site on a given day, conditional on that site being occupied by deer on that day. These included, in addition to an intercept (the baseline log density across all occupied sites in the study area), Julian day and Julian day squared (to accommodate non-linear, and potentially non-monotonic, temporal shifts in the overall number of deer within the study area), and the percent cover of forage vegetation (RAP-based grasses and forbs) in each site. To evaluate my hypotheses, I have additionally included NDVI and IRG values for each site on each day, as well as their interactions with grass and forb cover. These interactions reflect the notion that 'greenness' (as measured by NDVI) does not necessarily equate to forage quantity or quality – during the spring and early summer deer rely primarily on grasses and forbs and are thus expected to be responsive to the

greenness of those vegetation types. See table 2 for a full description of all parameters. The expected number of deer photos, given the site is occupied, can be written as:

$$\log(w_{i,t}) = \boldsymbol{X}_w \mathbf{B},$$

where $\boldsymbol{X}_w$ is the matrix of predictors and $\mathbf{B}$ is the vector of regression coefficients.

To accommodate both spatial and temporal autocorrelation, I estimated the distance-weighted effects of the previous day's density estimates on today's density estimate, based on a Gaussian spatial decay function (governed by a single free parameter, σ_x – its standard deviation), and a temporal linear operator (r, a free parameter between 0 and 1 defining the relative importance of the previous day's spatially integrated densities). I normalized the spatial decay so that the weight of site *i* was 1. That is, a site 0 distance away would have a weight of 1, and the weights would decay from there. I then multiplied each weight by the model-estimated number of photos at each site on the previous day (Nakashima et al. 2018). The spatiotemporal autocorrelation process can be written as:

$$x_{i,t} = \sum_{j=1}^{\Omega} N_{j,t-1} \cdot \exp\left(-\frac{|i-j|^2}{2 \cdot \sigma_x^2}\right),$$

where Ω is the total number of sites, $N_{j,t-1}$ is the model-estimated number of deer photos at site j at time $t-1$, and $|i-j|$ is the Euclidean distance between sites i and j.

Lastly, the probability that a deer present within a camera's detection zone was captured in a photo was modeled as a logit function of an intercept, α_p (baseline detectability), and site-level random effects around this intercept, η_i^p, with standard deviation σ_p:

$$logit(p_{i,t}) = \alpha_p + \eta_i^p,$$

$$\eta_i^p \sim Normal(0, \sigma_p).$$

The observed number of deer photos at site *i* at time *t* $(y_{i,t})$ is thus a binomial random variable, with $N_{i,t}$ trials and $p_{i,t}$ probability of success:

$$y_{i,t} \sim Binomial(N_{i,t}, p_{i,t}).$$

All variables were scaled and centred before model fitting. Models were fitted using an MCMC fitting procedure with weakly informative priors in R NIMBLE (de Valpine et al. 2017). Posterior estimates were obtained by running three independent chains for 70,000 iterations, and retaining the last 65,000 iterations as samples from the posterior (see Table 4 for resulting Gelman–Rubin convergence diagnostic). Models were fitted using R version 4.0.2 and NIMBLE version 0.10.1 (de Valpine et al. 2017). See Table 3 for all model parameters and prior specifications.

RESULTS

After removing questionable data resulting from the camera malfunctions described above, I retained 4,196 unique camera days between 15 March and 1 July, 2019. Cameras were active for mean = 62.6 days, SD = 30.2 days (Fig. 4). The 67 sites incorporated in this analysis ranged in elevation from 1,613 m to 2,559 m. Across 455,185 photos, I captured 12,792 deer observations. Other animals captured included cattle *(Bos taurus)*, sheep *(Ovis aries)*, elk *(Cervus canadensis)*, moose *(Alces alces)*, cougars *(Puma concolor)*, black bears *(Ursus americanus)*, coyotes *(Canis latrans)*, red foxes *(Vulpes vulpes)*, and turkeys *(meleagris gallopavo).*

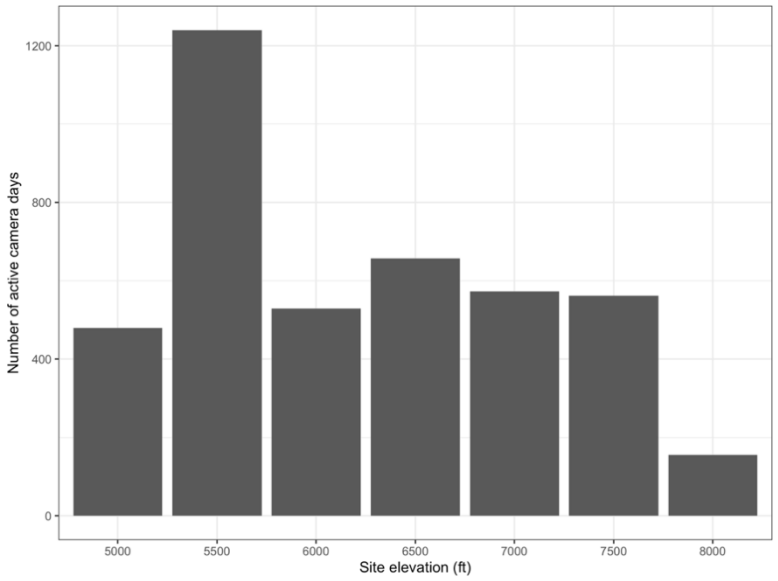

FIG 4. Number of active camera days across the entire study area by elevation. This distribution reflects the relative availability of elevation within the study area.

Probability of site occupancy across the entire study area decreased with Julian day (Table 1, γ_6), and Julian day^2 (γ_7). In combination with a negative effect of the interaction between elevation and Julian date (γ_4), and a positive effect of the interaction

between elevation and Julian day^2 (γ_5), these results are consistent with the expectation that probability of occupancy increases at higher elevations as the season progresses (Table 1, Figs. 5, 6). Additionally, my results indicate negative associations between deer occupancy and livestock presence (γ_2), snow presence (γ_3), and tree cover (γ_8). Lastly, probability of occupancy also varies substantially between sites, as indicated by the magnitude of the random effect (Fig. 9).

Table 1. Predictors for occupancy process $(z_{i,t})$ of the deer density model. Colons, e.g. as in 'Elevation:Julian', indicate an interaction between two predictor variables.

Coefficient	*Predictor*	*Units (before scaling and centering)*	*Posterior mean*	*90% CI*
γ_1	Intercept	unitless	-1.16	-1.55 ↔ -0.810
γ_2	Livestock presence	Present = 1; Absent = 0	-1.27	-2.20 ↔ -0.420
γ_3	Snow presence (MODIS)	Present = 1; Absent = 0	-0.642	-1.02 ↔ -0.257
γ_4	Elevation:Julian	m*days	-5.03	-6.41↔ -3.69
γ_5	Elevation:(Julian)^2	m*days^2	9.25	7.32 ↔ 11.2
γ_6	Julian	days	-4.25	-5.06 ↔ -3.44
γ_7	Julian^2	days^2	-1.33	-1.62 ↔ -1.04
γ_8	Tree cover (RAP)	%	-0.272	-0.464 ↔ -0.076

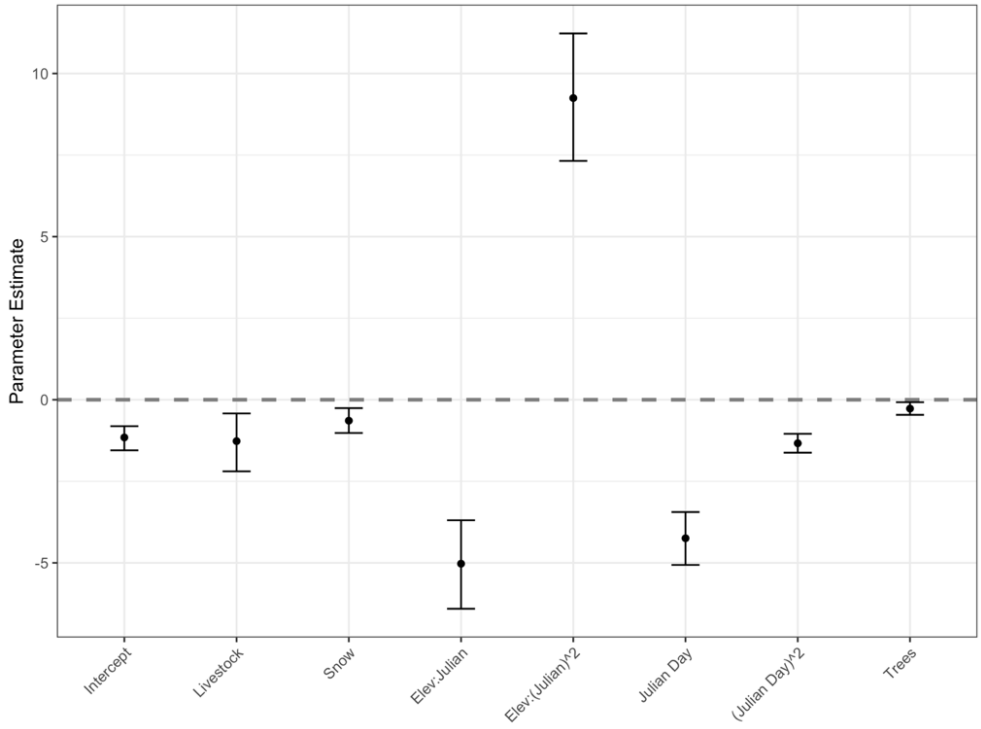

FIG 5. Posterior means for predictors in occupancy process. Bars denote 90% credible intervals.

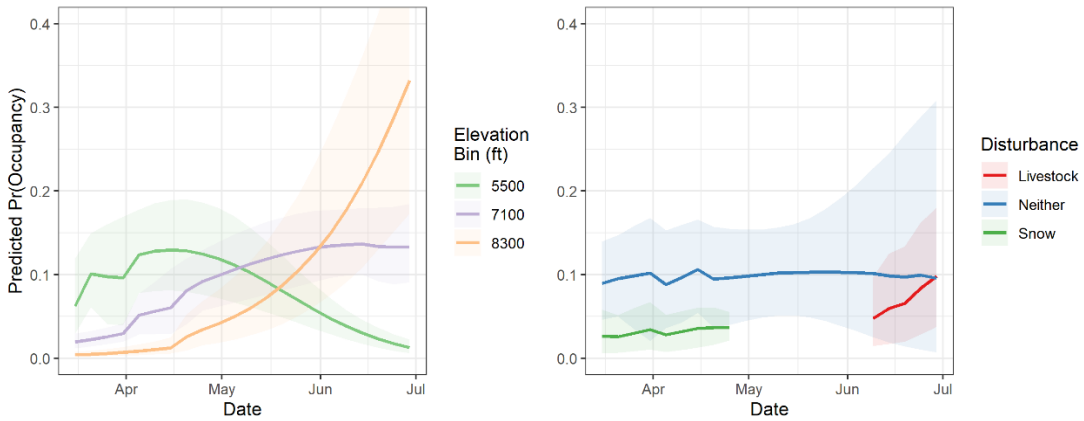

FIG 6. (Left) Predicted occupancy by date, sorted into elevation bins. Solid lines denote model-based relationship between date and site occupancy. Shaded region depict the corresponding 90% credible intervals. (Right) Predicted occupancy by date, sorted by disturbance levels (livestock, snow, or neither – snow and livestock were never observed on the same date). Solid lines denote model-based relationship between date and predicted occupancy, Shaded region depict the corresponding 90% credible intervals.

In the conditional abundance process (number of deer given that the site is occupied and detectability is 100%), I found negative effects of both Julian day (β_2) and Julian day^2 (β_3), indicating that, all other variables kept at their mean value, conditional deer density across the study area declines as the season progresses (amplifying the same trend in occupancy). Percent cover by grasses and forbs (β_4) had a positive effect on deer conditional density, as well as live green vegetation (NDVI, β_5). IRG alone (β_6) had no significant effect on abundance, however, when interacting with percent cover by grasses and forbs (β_8), IRG had a positive effect. By contrast, the interaction between NDVI and percent cover by grasses and forbs (β_7) had a negative effect. Combined, these results suggest that where herbaceous vegetation is scarce, deer selected for biomass availability (quantity), but in areas of abundant herbaceous vegetation (which deer generally preferred), selection shifts to focus on high growth rates (Table 2, Figs. 7, 8).

Table 2. Predictors for the count process $(w_{i,t}|z_{i,t} = 1)$ of the deer density model. This process is conditioned on the site being occupied. A colon, e.g., NDVI:(Grass+Forb), indicates an interaction between two predictor variables. NDVI = Normalized Difference Vegetation Index; IRG = Instantaneous Rate of Green-up.

Coefficient	*Predictor*	*Units (before scaling and centering)*	*Posterior mean*	*90% CI*
β_1	Intercept	unitless	3.54	3.36 ↔ 3.74
β_2	Julian	days	-0.223	-0.347 ↔ -0.121
β_3	Julian^2	days^2	-0.220	-0.290 ↔ -0.168
β_4	Grass + Forb Cover (RAP)	%	0.861	0.655 ↔ 1.07
β_5	NDVI (MODIS)	unitless	0.551	0.406 ↔ 0.727
β_6	IRG (MODIS)	unitless	-0.077	-0.205 ↔ -0.080
β_7	NDVI:(Grass+Forb)	%	-0.623	-0.793 ↔ -0.451
β_8	IRG:(Grass+Forb)	%	0.208	0.131 ↔ 0.282

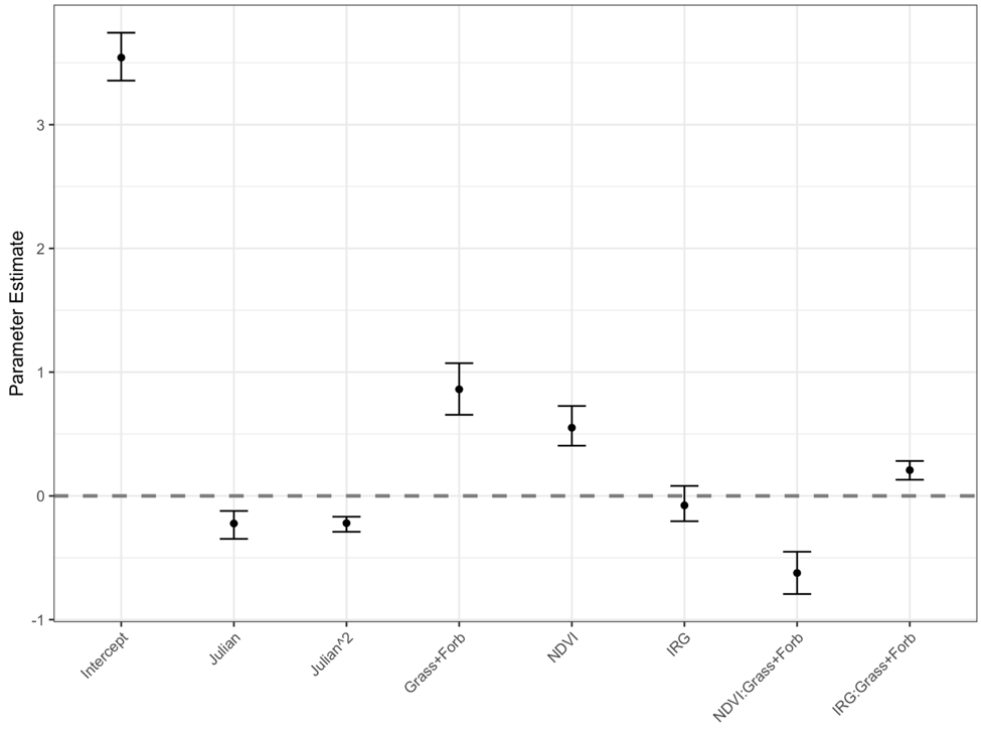

FIG 7. Posterior means for predictors in count process. Bars denote 90% credible intervals.

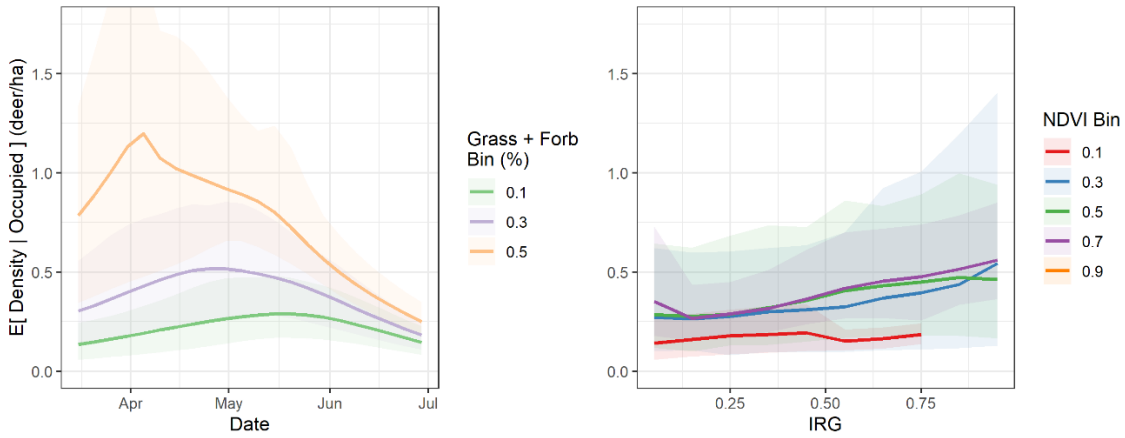

FIG 8. (Left) Predicted abundance given occupancy by date, sorted into bins based on percent cover by herbaceous vegetation (grass and forb species). Shaded region depict 90% credible intervals. (Right) Predicted density given occupancy by IRG, sorted into bins based on NDVI values. Shaded region depicts 90% credible intervals.

My results indicate that, on average, cameras captured approximately 25% of deer presence events within the field of view, but that detectability varied considerably across sites (Fig. 9). Spatiotemporal autocorrelation parameters indicate some support for contributions from surrounding area within several kilometres of the focal site, but negligible importance of these contributions in determining current deer densities, and hence, overall, weak spatiotemporal autocorrelations (Fig. 9).

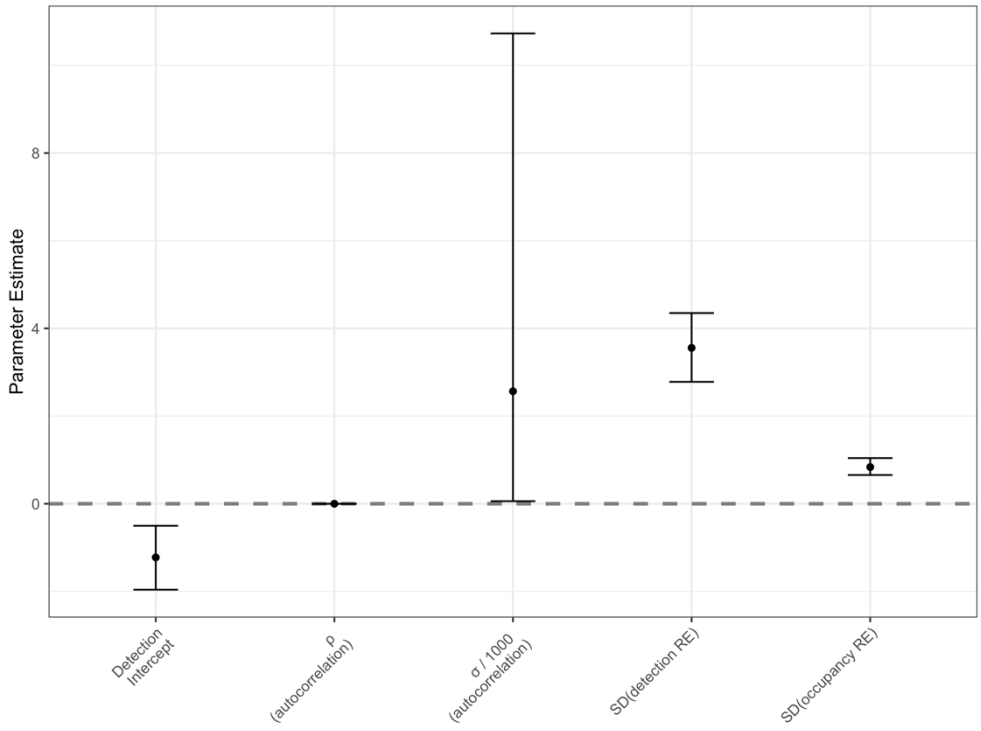

FIG 9. Posterior means for detection, autocorrelation, and random effects on detection and occupancy. Bars denote 90% credible intervals.

Integrating all of these various effects, I was able to generate predictive maps of deer densities across my entire study area and for any given day during the spring 2019 migration season (Fig. 10). Focusing on a specific date, the expected posterior deer densities in each site ($\rho_{i,t}$) were used to create an interpolated surface of deer densities

across the study area. Interpolations were achieved by ‘Co-Kriging’ (Krigging with covariates; using R package gstat) these posterior expected values while accounting for elevation and herbaceous vegetation cover. Below, I provide examples of these maps side by side with the concurrent NDVI and IRG raster.

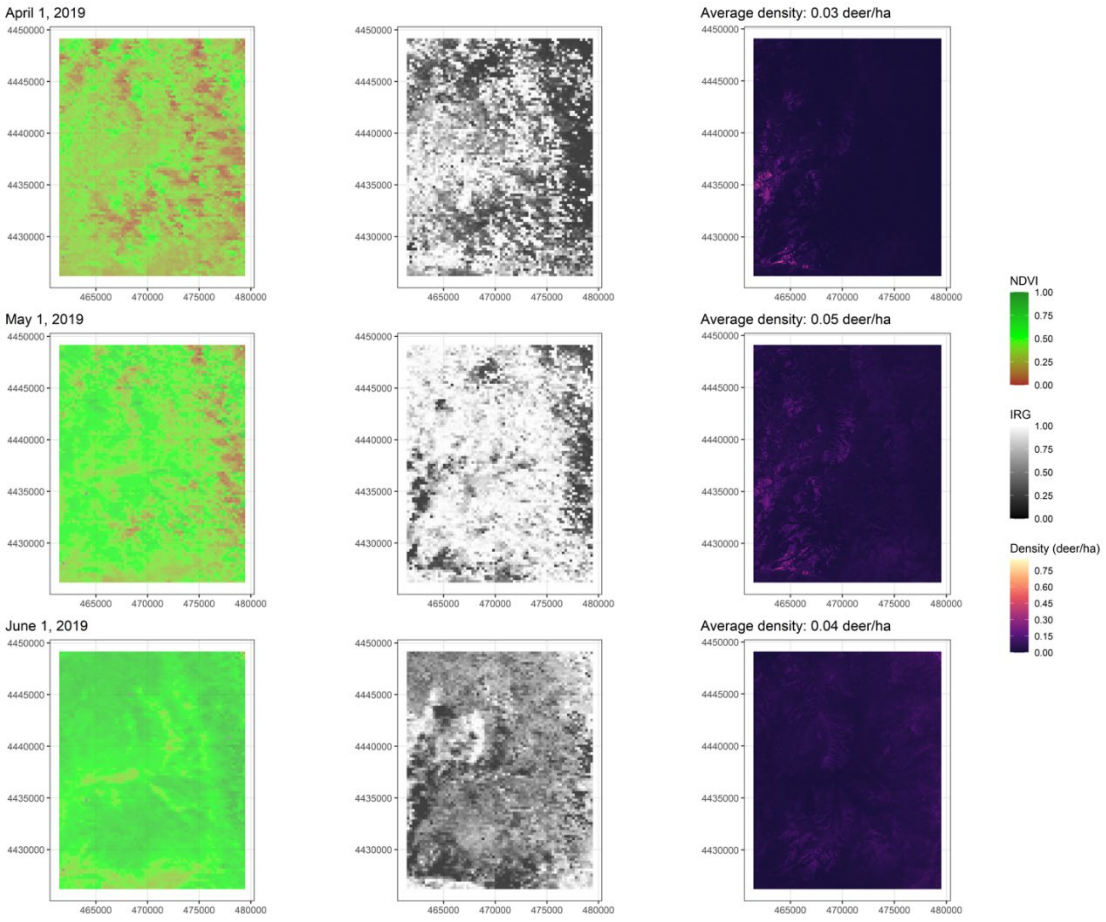

FIG 10. Maps of IRG and NDVI for three dates (early, mid, late spring season 2019) and corresponding predictive maps of deer density across the study area. Note the slight increase and then decrease of average deer density in the study area during the migratory season.

DISCUSSION

In this study, I was able to demonstrate, using novel field and statistical methodologies, support for population-level green-wave surfing in mule deer. This is the first demonstration of this phenomena at the population level, and confirms the hypothesis that vegetation growth is a driving force behind spring migration in our study system. I also found support for the hypothesis that forage quantity drives seasonal migration in my system, as deer density was positively correlated with biomass availability. Combined, these reinforce previous finding suggesting that 'green-wave surfing' may manifest as a compromise between maximising access to standing forage biomass (as captured by NDVI) and maximising access to forage growth (as captured by IRG; (Bischof et al. 2012, Merkle et al. 2016b). My findings thus support the notion that, not only is migration a means through which deer travel between seasonal ranges, it serves a functional role is replenishing nutritional resources after a metabolically intense winter season.

This demonstration of green-weave surfing from a Eulerian (population) perspective is of importance for ungulate species because it confirms patterns observed at the individual level in similar systems. Due to technological, financial, or logistical constrains, wildlife ecologists are often forced to make inferences about entire animal populations based on a small sample of individuals. For example, local biologists estimate that approximately 5,000 mule deer inhabit our study area, but we currently have location data for under 40 animals (which were all captured in the same, small area). Here, we were able to confirm that green wave surfing behavior is scalable to the

population level – a critical demonstration, because management and conservation targets often focus on population size, distribution, and health.

I was also able to investigate factors affecting deer occupancy at a fine spatiotemporal grain. Livestock presence had a negative effect on occupancy, suggesting interspecies competition for foraging resources (although I cannot rule out other negative interactions, such as competition for shade, increased vulnerability to predators, or increased exposure to parasites or micropredators). Snow also had a negative effect, likely a result of limited access for forage and impaired movement ability. I found that probability of occupancy at higher elevations increased with Julian date, above and beyond the effects of snow and forage, suggesting up-slope migration is driven by additional factors. Lastly, I found that deer in our study system were avoiding treed habitats, consistent with previous research demonstrating that coniferous cover (the dominant canopy cover in our study area) provides little nutritional benefit to deer (Serrouya and D'Eon 2008).

I was able to demonstrate the ability to create maps of projected deer distributions using empirical data. Because I characterized sampling sites using resources that can be projected across my entire study area, I was able to interpolate deer distributions across my entire study area (Fig. 10). Not only do these maps provide insight into ecological processes occurring in my system, they could be of significant utility in a management setting. Projected distributions could inform managers as to which habitat areas to prioritize, especially during critical life history periods (such as migration season). These predictive maps can provide insight into seasonal deer distribution patterns under different scenarios of vegetation growth. It has been demonstrated that global rates of

vegetation green-up are accelerating in pace and timing under the effects of anthropogenic climate change (Peng et al. 2017). In my system, this will lead to a narrower window of peak vegetation quality for migrating ungulates, with the possibility of phenological mismatch - both of which could have deleterious consequences on individual and herd health. In many systems, the effects of this acceleration could manifest as changes in the timing, duration, and location of migration routes of migratory deer. Using my model, biologists could use projected changes in vegetation growth to predict patterns of animal movement in coming years, and plan their management actions accordingly. Furthermore, I provide a transferable modeling framework that could be adapted to other study systems with animals that display similar migratory behavior, providing insight into animal distributions in herds that aren't currently monitored at the individual or population level.

Lastly, these projections provide mechanistically based, spatially integrated estimate of population density and its dynamics. Here, density was estimated to fluctuate from 0.03 deer/hectare in April, to 0.05 deer/hectare in May, down to 0.04 deer/ha in June. When I take the maximum obtained density throughout our study period and multiply that value by the size of our camera grid, we obtain a deer population of approximately 5,000 individuals – consistent with population size estimates by state wildlife biologists. As far as I know, this is the first demonstration that animal abundance could be reliably estimated by integrating over number of phots across extensive space and time.

The observed spatiotemporal fluctuation in density estimates makes sense when considering the geography of my study area. At the Northern and Southern ends of my

study area, cameras were situated primarily on summer (high-elevation) and winter (low-elevation) deer ranges (respectively). Most of my study areas however, and hence most cameras, were situated somewhere between these seasonal ranges, and hence capture the dynamics of deer density as the population undertakes its spring migration. As a result, deer density is observed to peak in mid season (when most deer have left their winter ranges, but have not yet completed their migration).

There were several caveats with using camera traps in this study. As mentioned earlier, our model estimated a low detection rate, and suggested that we were only capturing approximately 25% of deer presence events in front of our cameras. We conducted a series of controlled experiments and found that this estimate is realistic given the limitations of our trail cameras – across multiple trials, we found an average detection rate of 21% (see Appendix D for full details). We urge future studies to consider the specifications of their equipment in the context of study design, and to conduct adequate quality control and testing before deploying cameras in the field. Further, whereas the field methods used in this research allowed me to monitor wildlife densities at fine spatial and temporal grains and over large spatial and temporal extents., I have collected an extremely large dataset over the course of this study, and was actually unable to incorporate most of the data in the analysis presented here. Between the winter 2019 and fall 2020, I collected approximately 2,500,000 photos from 107 field sites. Whereas I had technicians manually tag the spring 2019 portion of this dataset (approximately 500,000 photos), I would urge future studies to investigate machine-learning methods to extract data from photos as a means to reduce the cost of conducting this type of research. A benefit of this rich dataset are the many opportunities for future research using this

dataset. I have documented the occurrence of many species (elk, moose, cougars, bears, and coyotes, among others) in the system, as well as potentially valuable information about vegetation and environmental conditions.

Building on these findings, it is still unknown whether the population-level patterns I have observed and quantified are consistent with individual movements in this system. As stated in the Introduction, simultaneous Lagrangian and Eulerian perspectives of the same processes are rare, and when available are not always in agreement due to variability in spatial and temporal sampling scales (Phillips et al. 2019). In future work I will investigate drivers of spring migration using individual-level telemetry data from deer in this study region, which will provide the first comparison of Eulerian and Lagrangian perspectives on spring migration in the same system.

In summary, in this study I was able to use emerging techniques in monitoring wildlife populations to observe Eulerian green-wave surfing behavior in migratory mule deer. I found support for the hypotheses that mule deer track vegetation growth and availability during the spring migration season, while gaining insight into other factors that affect habitat use. By utilizing the empirical results of my study, I was able to create spatially and temporally explicit maps of predicted deer density across a vast area, thus setting the stage for future advancements in Eulerian wildlife movement ecology.

LITERATURE CITED

Aikens, E. O., Kauffman, M. J., Merkle, J. A., Dwinnell, S. P. H., Fralick, G. L., and Monteith, K. L. 2017. The greenscape shapes surfing of resource waves in a large migratory herbivore. Ecology Letters, 20(6), 741–750. https://doi.org/10.1111/ele.12772

Aikens, E. O., Mysterud, A., Merkle, J. A., Cagnacci, F., Rivrud, I. M., Hebblewhite, M., … Kauffman, M. J. 2020. Wave-like Patterns of Plant Phenology Determine Ungulate Movement Tactics. Current Biology, 30(17), 3444-3449.e4. https://doi.org/10.1016/j.cub.2020.06.032

Albon, S. D., and Langvatn, R. 1992. Plant Phenology and the Benefits of Migration in a Temperate Ungulate. Oikos, 65(3), 502. https://doi.org/10.2307/3545568

Avgar, T., Street, G., and Fryxell, J. M. 2014. On the adaptive benefits of mammal migration. Canadian Journal of Zoology, 92(6), 481–490. https://doi.org/10.1139/cjz-2013-0076

Bischof, R., Loe, L. E., Meisingset, E. L., Zimmermann, B., Moorter, B. Van, and Mysterud, A. 2012. A Migratory Northern Ungulate in the Pursuit of Spring : Jumping or Surfing the Green Wave ?, 180(4), 407–424. https://doi.org/10.1086/667590

Boswell, A., Petersen, S., Roundy, B., Jensen, R., Summers, D., and Hulet, A. 2017. Rangeland monitoring using remote sensing: comparison of cover estimates from field measurements and image analysis. AIMS Environmental Science, 4(1), 1–16. https://doi.org/10.3934/environsci.2017.1.1

Burton, A. C., Neilson, E., Moreira, D., Ladle, A., Steenweg, R., Fisher, J. T., … Boutin, S. 2015. Wildlife camera trapping: A review and recommendations for linking surveys to ecological processes. Journal of Applied Ecology, 52(3), 675–685. https://doi.org/10.1111/1365-2664.12432

Couturier, S., Cŏté, S. D., Huot, J., and Otto, R. D. 2009. Body-condition dynamics in a northern ungulate gaining fat in winter. Canadian Journal of Zoology, 87(5), 367–378. https://doi.org/10.1139/Z09-020

de Valpine, P., Turek, D., Paciorek, C. J., Anderson-Bergman, C., Lang, D. T., and Bodik, R. 2017. Programming With Models: Writing Statistical Algorithms for General Model Structures With NIMBLE. Journal of Computational and Graphical Statistics, 26(2), 403–413. https://doi.org/10.1080/10618600.2016.1172487

Fryxell, J. M., and Sinclair, A. R. E. 1988. Causes and consequences of migration by

large herbivores. Trends in Ecology and Evolution, 3(9), 237–241. https://doi.org/10.1016/0169-5347(88)90166-8

Garland, L., Neilson, E., Avgar, T., Bayne, E., and Boutin, S. 2020. Random Encounter and Staying Time Model Testing with Human Volunteers. Journal of Wildlife Management, 84(6), 1179–1184. https://doi.org/10.1002/jwmg.21879

Hebblewhite, M., Merrill, E., and McDermid, G. 2008. A Multi-Scale Test Of The Forage Maturation Hypothesis In A Partially Migratory Ungulate Population. Ecological Monographs, 78(2), 141–166. https://doi.org/10.1890/06-1708.1

Kays, R., Arbogast, B. S., Baker-Whatton, M., Beirne, C., Boone, H. M., Bowler, M., … Spironello, W. R. 2020. An empirical evaluation of camera trap study design: How many, how long and when? Methods in Ecology and Evolution, 11(6), 700–713. https://doi.org/10.1111/2041-210X.13370

Lendrum, P. E., Anderson, C. R., Monteith, K. L., Jenks, J. A., and Bowyer, R. T. 2014. Relating the movement of a rapidly migrating ungulate to spatiotemporal patterns of forage quality. Mammalian Biology, 79(6), 369–375. https://doi.org/10.1016/j.mambio.2014.05.005

Long, R. A., Kie, J. G., Terry Bowyer, R., and Hurley, M. A. 2009. Resource selection and movements by female mule deer Odocoileus hemionus: Effects of reproductive stage. Wildlife Biology, 15(3), 288–298. https://doi.org/10.2981/09-003

Martin, A. P., Zubkov, M. V., Burkill, P. H., and Holland, R. J. 2005. Extreme spatial variability in marine picoplankton and its consequences for interpreting Eulerian time-series. Biology Letters, 1(3), 366–369. https://doi.org/10.1098/rsbl.2005.0316

Meek, P. D., Ballard, G., Claridge, A., Kays, R., Moseby, K., Sanderson, J., … Townsend, S. 2014. on camera trapping research. https://doi.org/10.1007/s10531-014-0712-8

Merkle, J. A., Monteith, K. L., Aikens, E. O., Hayes, M. M., Hersey, K. R., Middleton, A. D., … Kauffman, M. J. 2016a. Large herbivores surf waves of green-up during spring, 1–8.

Merkle, J. A., Monteith, K. L., Aikens, E. O., Hayes, M. M., Hersey, K. R., Middleton, A. D., … Kauffman, M. J. 2016b. Large herbivores surf waves of green-up during spring. Proceedings of the Royal Society B: Biological Sciences, 283(1833), 1–8. https://doi.org/10.1098/rspb.2016.0456

Middleton, A. D., Merkle, J. A., McWhirter, D. E., Cook, J. G., Cook, R. C., White, P. J., and Kauffman, M. J. 2018. Green-wave surfing increases fat gain in a migratory

ungulate. Oikos, 127(7), 1060–1068. https://doi.org/10.1111/oik.05227

Monteith, K. L., Bleich, V. C., Stephenson, T. R., Pierce, B. M., Conner, M. M., Klaver, R. W., and Bowyer, T. 2011. Timing of seasonal migration in mule deer: Effects of climate, plant phenology, and life-history characteristics. Ecosphere, 2(4), 1–34. https://doi.org/10.1890/ES10-00096.1

Nakashima, Y., Fukasawa, K., and Samejima, H. 2018. Estimating animal density without individual recognition using information derivable exclusively from camera traps. Journal of Applied Ecology, 55(2), 735–744. https://doi.org/10.1111/1365-2664.13059

Nandigam, V., and Fergraus, E. 2018. Wild.ID (Version 0.0.31) [Computer Software]

Nicholson, M. C., Terry Bowyer, R., and Kie, J. G. 1997. Habitat selection and survival of mule deer: Tradeoffs associated with migration. Journal of Mammalogy, 78(2), 483–504. https://doi.org/10.2307/1382900

Peng, D., Wu, C., Li, C., Zhang, X., Liu, Z., Ye, H., … Fang, B. 2017. Spring green-up phenology products derived from MODIS NDVI and EVI: Intercomparison, interpretation and validation using National Phenology Network and AmeriFlux observations. Ecological Indicators, 77, 323–336. https://doi.org/10.1016/j.ecolind.2017.02.024

Pettorelli, N., Gaillard, J. M., Yoccoz, N. G., Duncan, P., Maillard, D., Delorme, D., … Toïgo, C. 2005. The response of fawn survival to changes in habitat quality varies according to cohort quality and spatial scale. Journal of Animal Ecology, 74(5), 972–981. https://doi.org/10.1111/j.1365-2656.2005.00988.x

Phillips, E. M., Horne, J. K., Zamon, J. E., Felis, J. J., and Adams, J. 2019. Does perspective matter? A case study comparing Eulerian and Lagrangian estimates of common murre (Uria aalge) distributions. Ecology and Evolution, 9(8), 4805–4819. https://doi.org/10.1002/ece3.5083

Robbins, C. T., and Hanley, T. A. 2016. Energy Expenditures for Locomotion by Mule Deer and Elk Author (s): Katherine L . Parker , Charles T . Robbins and Thomas A . Hanley Published by : Wiley on behalf of the Wildlife Society Stable URL : http://www.jstor.org/stable/3801180 Accessed : 15-03, 48(2), 474–488.

Rovero, F., Zimmermann, F., Berzi, D., and Meek, P. 2013. “Which camera trap type and how many do I need?” A review of camera features and study designs for a range of wildlife research applications. Hystrix, 24(2), 148–156. https://doi.org/10.4404/hystrix-24.2-6316

Rowcliffe, J. M., Field, J., Turvey, S. T., Carbone, C., Turvey, T., and Nw, L. 2008. Estimating animal density using camera the need for individual recognition traps

without. Journal of Applied Ecology, 45(4), 1228–1236. https://doi.org/10.1111/j.l365-2664.2008.01473.x

Sawyer, H., Lindzey, F., and McWhirter, D. 2005. Mule deer and pronghorn migration in western Wyoming. Wildlife Society Bulletin, 33(4), 1266–1273. https://doi.org/10.2193/0091-7648(2005)33[1266:mdapmi]2.0.co;2

Serrouya, R., and D'Eon, R. G. 2008. The influence of forest cover on mule deer habitat selection, diet, and nutrition during winter in a deep-snow ecosystem. Forest Ecology and Management, 256(3), 452–461. https://doi.org/10.1016/j.foreco.2008.04.048

The National Map. (n.d.). Retrieved December 3, 2020, from https://www.usgs.gov/core-science-systems/national-geospatial-program/national-map

Turchin, P. 2015. *Quantitative Analysis of Movement: Measuring and Modeling Population Redistribution in Animals and PlantsTitle*. Beresta Books.

APPENDICES

APPENDIX A. SUPPLEMENTARY TABLES

Table 3. All parameters and priors for the deer density model. Note that all Normal distributions are parameterized by (mean, SD). $T(0,)$ indicates that the probability distribution was left truncated at 0.

Parameter	*Description*	*Prior*
r	Strength of autocorrelation	$Beta(1,1)$
σ_x	Decay of spatial autocorrelation weights	$Normal(10\,000, 10\,000)\ T(0,)$
$\gamma_{1:8}$	Regression coefficients for occupancy process $(z_{i,t})$	$Normal(0,10)$
$\beta_{1:8}$	Regression coefficients for count process given occupancy $(w_{i,t}\|z_{i,t}=1)$	$Normal(0,10)$
α_1	Intercept of detection process $(p_{i,t})$	$Normal(0,1)$
σ_ψ	Standard deviation of random effect for the occupancy process $(z_{i,t})$	$Normal(1,1)\ T(0,)$
σ_p	Standard deviation of random effect for the detection process $(p_{i,t})$	$Normal(1,1)\ T(0,)$

Table 4. Gelman-Rubin convergence diagnostic. MPSRF = 9.01.

Coefficient	*Predictor/Description*	*PSRF point est.*	*Upper CI*
β_1	Intercept	6.07	11.61
β_2	Julian	3.09	5.66
β_3	Julian^2	3.47	6.36
β_4	Grass + Forb Cover (RAP)	1.57	2.41
β_5	NDVI (MODIS)	1.09	1.27
β_6	IRG (MODIS)	1.69	2.68
β_7	NDVI:(Grass+Forb)	1.26	1.72
β_8	IRG:(Grass+Forb)	1.14	1.41
γ_1	Intercept	1.74	2.78
γ_2	Livestock presence	1.44	2.14
γ_3	Snow presence (MODIS)	1.26	1.70
γ_4	Elevation:Julian	1.14	1.43
γ_5	Elevation:(Julian)^2	1.20	1.57
γ_6	Julian	1.39	2.01
γ_7	Julian^2	1.11	1.32
γ_8	Tree cover (RAP)	1.07	1.23
r	Strength of autocorrelation	1.00	1.01
σ_x	Decay of spatial autocorrelation weights	1.34	2.46
α_1	Intercept of detection process $(p_{i,t})$	1.21	1.58
σ_ψ	Standard deviation of random effect for the occupancy process $(z_{i,t})$	1.45	2.15
σ_p	Standard deviation of random effect for the detection process $(p_{i,t})$	1.83	2.98

APPENDIX B. FULL CAMERA DEPLOYMENT PROTOCOLS

We used Cuddeback H-1453 and Reconyx HP2X cameras to capture images of large terrestrial wildlife at our field sites. Exact camera settings varied with camera model, but in all cases, they were programmed to take continuous photos as long as motion was detected in their field of view. Sensitivity settings were set to the highest possible option, with no daily 'quiet' or dormant periods. Cameras and SD cards were all assigned unique numerical IDs and labelled appropriately.

Although our camera placements were random, potential field sites had to meet several qualifications. Sites needed to be fairly level (to allow for adequate camera view), set back from obvious roads and trails to prevent human tampering/theft, and needed to be accessible in variable seasonal weather conditions (for example, not across rivers that would flood in the spring time). The sites needed to have an immediate area that was clear of dense trees/shrubs that could obstruct the camera's field of view, although they typically had fence posts/trees that the camera units themselves were mounted on (at a couple sites, cameras were mounted on rebar that we staked into the ground). After a suitable mounting object was identified, vegetation/branches were cleared from the immediate vicinity of the camera to prevent false-positive images generated by vegetation moving in the wind. Generally, we avoided placing cameras facing directly East or West to avoid sun glare in photos taken around sunrise or sunset. Cameras were screwed into trees/fence posts at a height of 1 m from ground to the base of the camera lens using a combination of wood screws, metal plumber's tape, and manufacturer-provided camera mounts. In snowy conditions, a snow measurement probe was used to confirm mounting height.

Once cameras were mounted, we delineated our sampling area using sections of pre-cut metal conduit staked into the ground. These markers were 13mm in diameter, 1.5m, and driven 0.2m into the ground at 3 designated locations. One of the markers was placed 20 ft in front of the camera, at the center of the camera's field of view. Two additional markers were then placed 20 ft from the camera, but at an angle of 15 degrees from the center line – one 15 degrees east, the other 20 degrees west (see Fig. 11).

After cameras and conduits were deployed, we confirmed the camera's field on view via two methods. First, we used the built-in 'walk test' function on the cameras, designed to flash a light if they detect motion in the field of view, and had technicians walk a series of transects in front of the conduit markers to be sure the cameras were registering motion in our delineated study area. Next, we triggered the cameras to take a site photos, then used an adapter to view the captured picture on a smartphone. This enabled us to verify that the conduit markers would be visible in naturally-triggered photos.

Cameras were re-visited in late summer 2019, when we collected photos taken during the spring 2019 migration season. At this time, we also conducted a site-level vegetation survey, as described in Appendix C.

APPENDIX C. GROUND TRUTHING RAP VEGETATION COVER DATA

Field surveys were conducted at each camera site in early summer to characterise vegetation type and structure. These vegetation protocols were developed in consideration of the Utah Division of Wildlife's range trend survey protocols, which are used to evaluate habitat suitability for big game species throughout the state. Survey data provide temporally static, detailed information on local forage composition at the camera's immediate vicinity. A 33 m measuring tape was placed perpendicular to the camera field of view, 9 m away from the camera, centered at the middle conduit marker. A secondary 33 m measuring tape was placed directly in the camera field of view, beginning at the camera itself and extending away from the camera. A line intercept survey was conducted along both transects, where the observer traveled along the tapes and recorded (in centimeters) each vegetation and cover class directly intersecting the transects. Cover classes recorded included graminoids, forbs, litter, cryptograms, bare ground, rock, unknown shrubs, juniper, sagebrush, scrub oak, cactus, maple, aspen, unknown trees, and water. If a cover class intercepted the line for less than 15 cm, it was not counted. Percent cover was then calculated by dividing the length of each cover class observed by the total line intercept distance surveyed at each site.

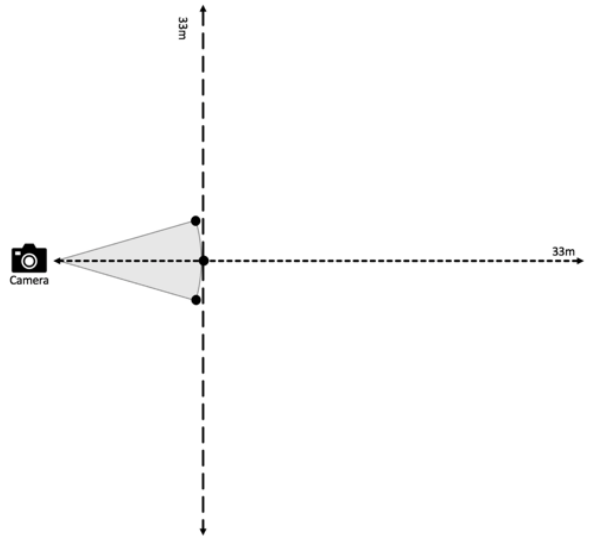

FIG 11. Diagram of vegetation survey transects conducted at field sites. Line intercept surveys were conducted along short – and long-dashed lines.

Survey information was compared to the NRCS/BLM's Rangeland Analysis Platform (RAP 2) dataset, which was used to characterize vegetation composition at sites in this analysis (Boswell et al. 2017). RAP data provided annual percent cover estimates using a composite of BLM Assessment, Inventory, and Monitoring (AIM) surveys, NRCS National Resources Inventory (NRI) surveys, and LANDSAT satellite imagery (Boswell et al. 2017). Importantly, while RAP data has only a 30 m, annual spatiotemporal resolution, it can be derived for any location in Western US and for any year since 1984. Consequently, reliance on RAP data instead of on our ground surveys allows both interpolation of our results within our study area, and extrapolation outside of the study area and period.

RAP cover classes are more coarsely aggregated than those that we classified in site surveys (annual and perennial grasses and forbs, trees, shrubs, bare ground, and litter). In order to compare our two sources of site vegetation composition, we collapsed

RAP data into 3 categories – bare ground and litter, trees and shrubs, and grasses and forbs. Similarly, we collapsed our surveys classes into a graminoid/forbs class (graminoids, forbs, and cactus combined), a tree/shrub class (unknown trees, unknown shrubs, aspens, maples, scrub oaks, sagebrush, and juniper), and a bare ground class (rock, bare ground, cryptogram, litter, and water). Scatterplots below illustrate the relationship between RAP and site survey data for each of the collapsed cover classes, with each point representing a unique site. Boxplots demonstrate site composition according to RAP and survey data.

As shown in Fig. 12, we found that RAP percent cover data is positively and linearly correlated with our site-level ground survey data. Unsurprisingly, our finer scale observations are more variable (notably for grass and forbs), but the two data sets are in agreement as to the relative abundance of different cover classes across our study area (Fig. 13). Overall, we found that this comparison indicated that RAP data provides an adequate characterization of vegetation cover in our study area, while allowing us to interpolate outside our study sites and sampling period.

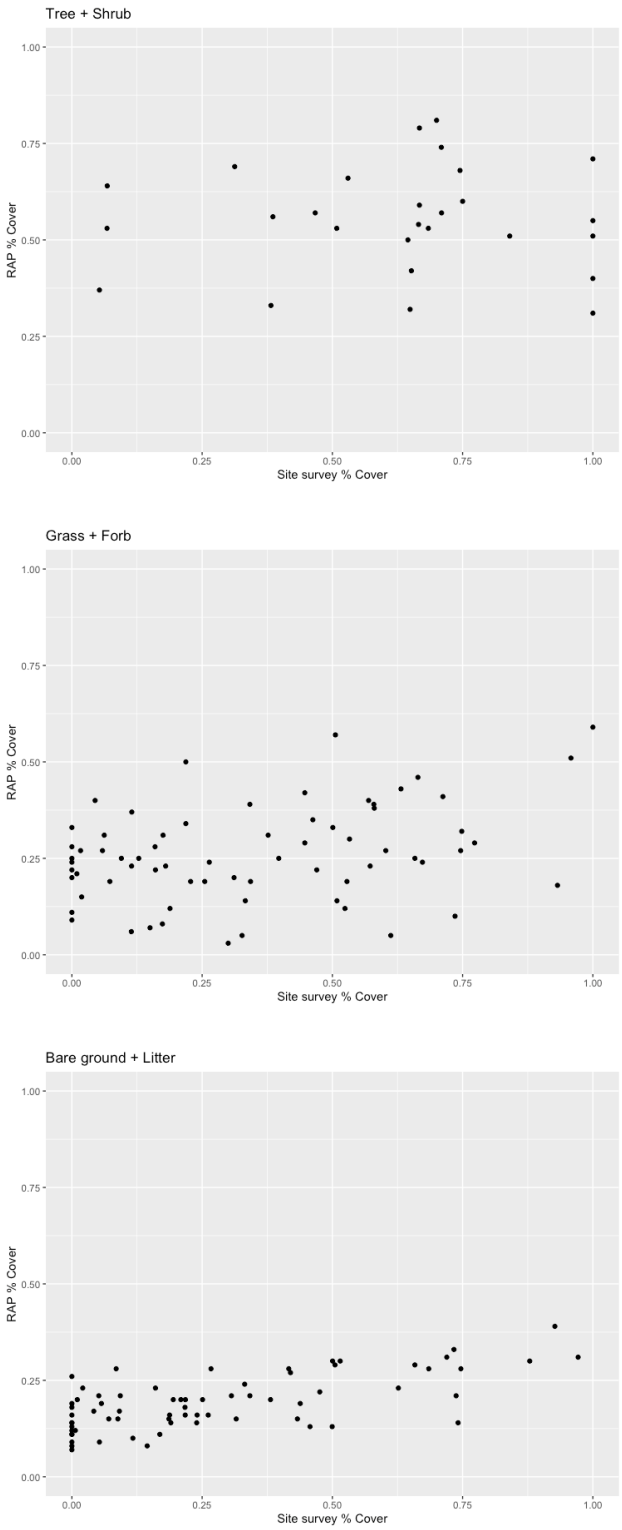

FIG 12. Scatterplot comparisons of percent cover collected from RAP and site-level vegetation surveys, by cover class category.

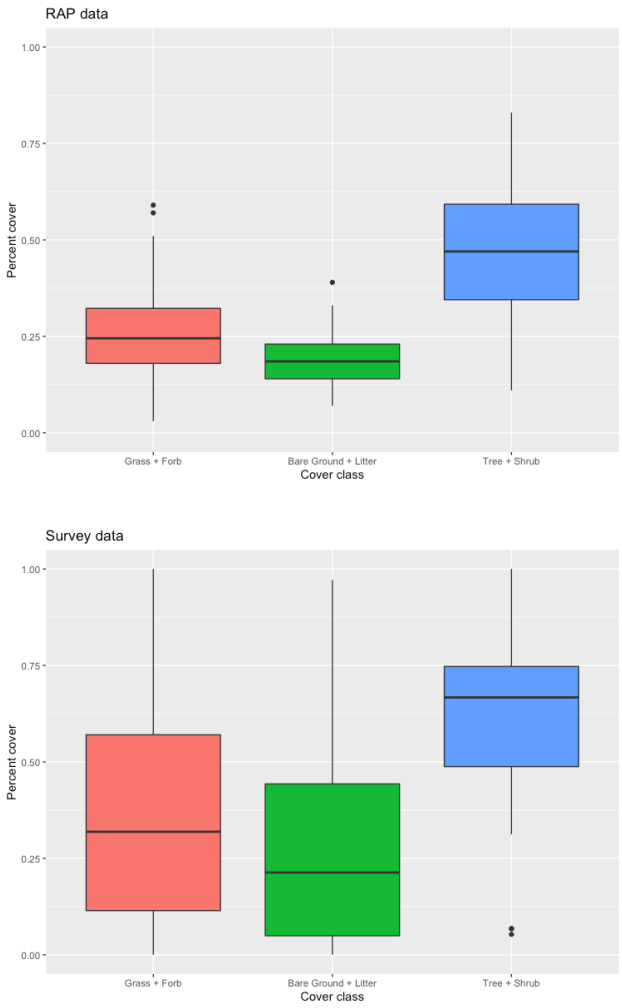

FIG 13. Comparison of RAP vs site survey percent cover data across entire study area.

APPENDIX D. DETECTION RATE TESTING

In order to better understand the limitations of our camera setups, we conducted a series of trials designed to evaluate camera detection rates in a controlled setting. We tested both models of camera used in our study (Cuddeback H-1453 and Reconyx HP2X units) by walking 30 m wide transects located at distances of 3, 6, 9, 12, 15, and 18 m from the camera units. We were also interested in how captures rates would vary with animal movement speed, so we walked our transects at two different speeds ('fast' 'slow', which equated to ~7.5 km/hr and 3.75 km/hr, respectively). Cameras were mounted and programmed in the same fashion as in the field, at a height of 1 m from the ground on a tree, and transects were centered and perpendicular to the cameras.

Each transect was walked 3 times at each speed, meaning 72 total walking trials were conducted (2 camera models, 2 speeds, 6 transect distances, 3 walking trials each). We recorded the amount of time the technician spent walking each transect, and the number of photos captured on each transect walk. Each photo was taken to represent 2 seconds of 'detection', as this was the camera recovery rate, and we then divided the number of detection seconds by the total amount of time spent walking each transect. Overall, our cameras were abysmal at capturing photos. Across all transect distances, camera models, and walking speeds, our average 'detection rate' was 20.8%. This varied by camera model (with Reconyx units performing better), distance (with peak 'detection' occurring at an intermediate distance), and walking rate (with slower speeds lending towards higher detection), but overall we found that our modeled detection rate of ~25% to be consistent with the results in this small, controlled experiment (Fig. 14).

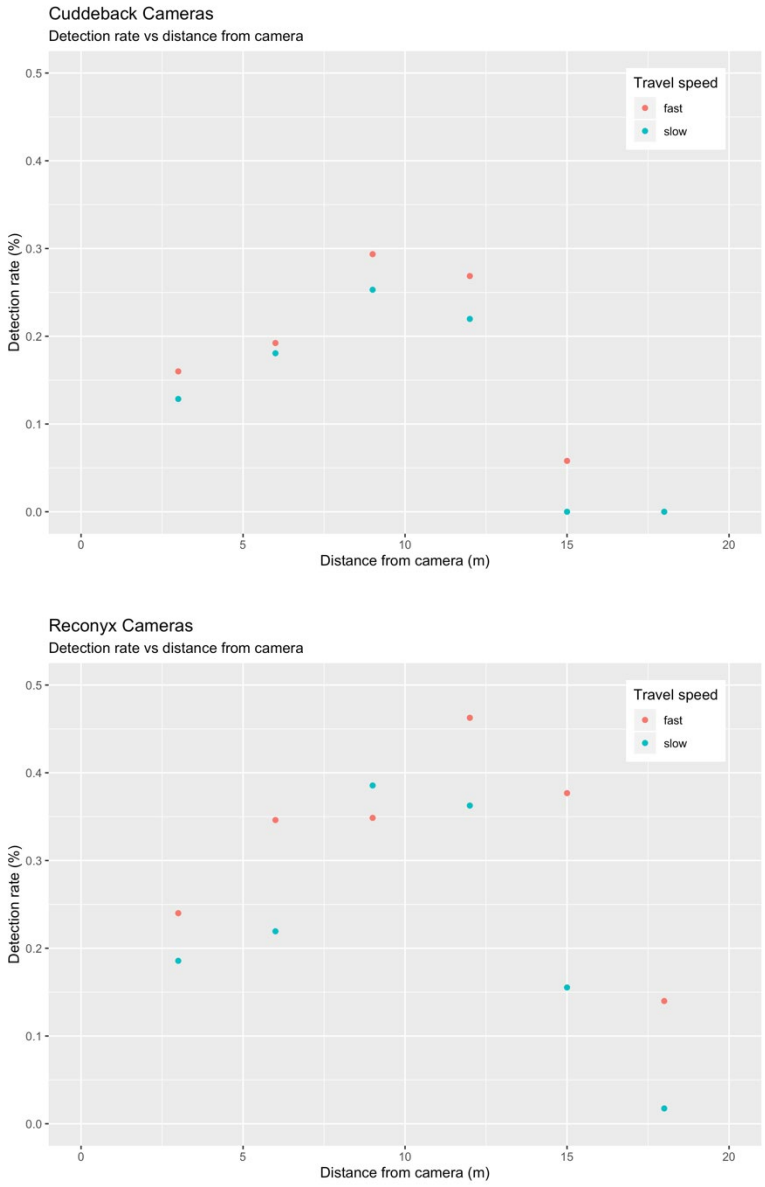

FIG 14. Comparison of camera detection rates in a controlled environment, sorted by camera type, travel speed and distance of movement from camera.